EBIC characterization of strained Si/SiGe heterostructures

© E.B. Yakimov¶, R.H. Zhang*, G.A. Rozgonyi*, M. Seacrist†

Institute of Microelectronics Technology and High Purity Materials, Russian Academy of Sciences,
142432 Chernogolovka, Russia
* Department of Materials Science and Engineering, North Carolina State University,
27695 Raleigh, North Carolina, USA
† MEMC Electronic Materials,
MO 63376 St. Peters, USA

(Получена 12 сентября 2006 г. Принята к печати 3 октября 2006 г.)

Strained-Si/SiGe heterostructure is studied by the EBIC. The effect of annealing at 800°C is investigated. The EBIC images obtained at different beam energies are analyzed. The analysis of images obtained shows that misfit dislocation bunches in the graded SiGe layer could not explain the cross-hatch contrast dependence on E_b. Therefore, at least a part of this contrast should be associated with other defects located closer to the depletion region. It is assumed that dislocation trails could play a role of such defects.

PACS: 68.37.Hk, 72.80.Cw

1. Introduction

Strained Si is a promising candidate to replace traditional bulk Si in the high-speed complementary metal-oxide-semiconductor (CMOS) technology, due to the higher electron and hole mobilities in the strained-Si channel layer [1]. In a typical device structure, the strained Si layer is grown on the virtual SiGe substrate, which consists of the uniform and compositionally graded SiGe layers on a highly doped Si substrate. The strain relaxation during the virtual substrate manufacturing results in formation of misfit dislocations in the graded SiGe layer and the threading dislocations running up from this layer towards the top of the structure. The density of these threading dislocations, which are inherited by the growing strained Si layer, usually exceeds $10^5-10^6\,\mathrm{cm}^{-2}$. The strained Si layer with a thickness exceeding the critical one [2,3] is metastable against the dislocation formation. Therefore, a partial strain relaxation could occur during subsequent thermal processing resulting in formation of the misfit dislocations at the strained-Si/SiGe interface. The misfit and threading dislocations in the strained Si layer can essentially affect the device performance [4–6]. An additional factor affecting the device performance is the cross-hatching, a large-scale roughness inherent in such structures due to the stress fields associated with the underlying misfit dislocations generated during relaxation in the graded SiGe layer [7].

Therefore, it is crucial to carefully explore the distribution, electrical properties and thermal stability of defects created during stress relaxation. The Electron Beam Induced Current (EBIC) technique is well suited for such investigation [8,9]. It has been shown [4,10,11] that this method allows to detect misfit dislocations in the graded SiGe and threading dislocations. At low beam energy the contrast inside the depletion region was observed [10,11], which was ascribed to misfit dislocations near strained Si/SiGe interface. However, recent investigations of individual dislocations in clean Si wafers [12–14] showed that their EBIC contrast was negligible. In the same time the electrically active defects can be formed behind moving dislocations (dislocation trails), which could produce the rather strong EBIC contrast even in clean crystals [13–15]. Therefore, the question about the nature of EBIC contrast observed in Si/SiGe heterostructures seems to be not totally closed. To clarify this point the additional investigations are necessary.

In the present paper, the metastable strained-Si/SiGe heterostructure has been studied by the EBIC technique. The EBIC images obtained at different beam energies are analyzed. The effect of annealing at 800°C is investigated.

2. Experimentals

The strained-Si/SiGe/Si-substrate heterostructure was grown by chemical vapour deposition on a *p*-type 200 mm Si wafer using either SiH_4 (for strained-Si layer) or SiH_2Cl_2 and GeH_4 (for SiGe layer) as source gases. The structure consists of four epilayers deposited on a highly doped *p*-Si substrate with a boron concentration of about $10^{19}\,\mathrm{cm}^{-3}$. On the Si wafer, a 2500 nm thick Si epilayer of $10^{16}\,\mathrm{cm}^{-3}$ boron doping was grown, which is followed by a 670 nm thick graded $Si_{1-x}Ge_x$ layer (x is increased from 0 to 20%), and a 1000 nm thick uniform $Si_{1-x}Ge_x$ ($x = 20\%$). Finally, a strained-Si layer with a thickness of 73.5 nm was grown on the relaxed uniform SiGe layer. As-grown strained-Si/SiGe heterostructure was divided into two parts, and one of them was annealed at 800°C in oxidizing atmosphere to grow a 10 nm thick oxide to represent the conventional gate oxide growth process. Since the 73.5 nm strained-Si layer is larger than the calculated critical thickness (~ 25 nm) for strained Si grown on relaxed $Si_{0.8}Ge_{0.2}$ [2,3], the as-grown top Si layer was metastable, and it could undergo some relaxation during thermal annealing.

The EBIC studied were performed using a JSM-840A (JEOL) SEM operating in the EBIC mode at electron-beam (*e*-beam) energy E_b varying from 8 to 30 keV and

¶ E-mail: yakimov@ipmt-hpm.ac.ru

at temperatures of 90 and 300 K. The Schottky and ohmic contacts were prepared by evaporating Al on the strained-Si layer surface, and by rubbing Ga–In on the backside, respectively. Thermally grown oxide on the annealed sample was removed using a diluted HF solution before preparing the Schottky contacts. The effective diffusion length L is estimated by fitting the measured collection efficiency dependence β on beam energy E_b by calculated one. As usually [9], the collection efficiency β is determined as $\beta = \frac{I_c E_i}{I_b E_b \eta}$, where I_c is the collected current, I_b is the beam current, η is the beam energy absorption coefficient and E_i is the energy necessary for electron–hole pair creation (3.6 eV for Si). The defect contrast in the EBIC micrographs is determined as $C = 1 - I_{\text{dark}}/I_{\text{br}}$, where I_{dark} and I_{br} are the collected current values in the dark and bright regions, respectively. The minimum contrast, which could be revealed by the system used is of about 0.5%.

3. Experimental results and discussion

To extract the defects properties from the EBIC measurements two approaches could be used. The first one is based on the diffusion length measurements that allows to estimate the total recombination rate associated with defects under study. And the second one is based on the EBIC image analysis and allows to reveal individual extended defects, to estimate their density, location and recombination activity. The effective diffusion length in the structure studied was estimated by fitting the collected efficiency dependence on E_{b}. The experimental dependence measured on the annealed sample together with simulated one is presented in Fig. 1. It is seen that the dependence calculated using the effective diffusion length $L = 5\,\mu$m fits rather well the measured one. For as-grown samples the similar L value was obtained by fitting. The obtained from fitting effective depletion region width, i.e. the region with a high enough electric field, where carrier drift prevails over their diffusion, was of about $0.4\,\mu$m that well correlated with a value obtained from $C-V$ measurements.

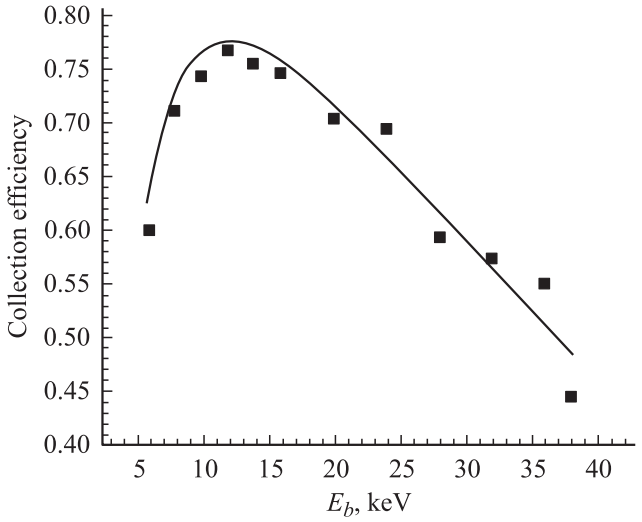

Figure 1. The collection efficiency dependence on E_b for annealed sample. The simulated dependence was shown by solid line.

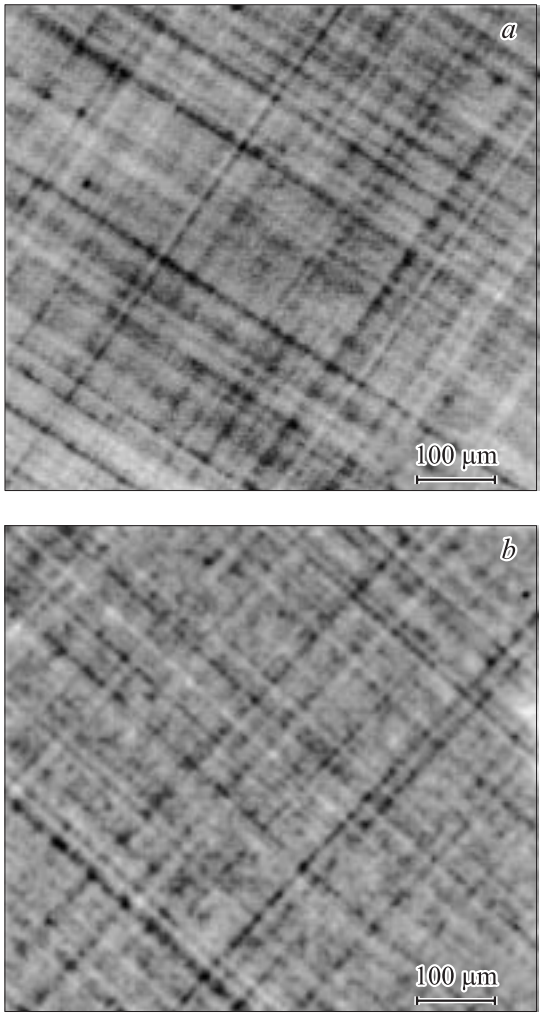

Figure 2. EBIC images of as-grown (a) and annealed (b) samples obtained at 90 K and $E_b = 20$ keV.

The structure under study consists of a few layers with different properties therefore their effect on the obtained L value should be estimated. Calculation of collection efficiency for a model structure consisting of a few layers with varied diffusion length showed that the recombination inside the constant SiGe layer produced the negligible effect on the measured L due to the large enough effective depletion region width and large L. Thus, to fit the experimental dependence the recombination inside the only two layers: the graded SiGe layer and the highly doped Si substrate could be considered. The experimental dependence could be fitted rather well using different combinations of diffusion length values in these two layers. However, to fit the experimental dependence the diffusion length in the substrate could not be smaller than $5\,\mu$m and in this case the diffusion length inside the graded SiGe layer

should be also of about $4-5\,\mu$m. If the diffusion length in the substrate is assumed to be larger than $20\,\mu$m the measured dependence could be fitted under an assumption that the diffusion length inside the graded SiGe layer is of about $1.5\,\mu$m. Thus, such fitting allows to estimate the diffusion length inside the graded SiGe layer and shows that Si substrate could noticeable affects the effective L value. As follows from such estimations, the diffusion length inside the graded SiGe layer should be in the range from 1.5 to $5\,\mu$m.

The EBIC images obtained at beam energies E_b larger than 10 keV demonstrate two-dimensional cross-hatch pattern consisting of dark and bright bands ($5-10\,\mu$m wide), which is qualitatively similar in both as-grown and annealed heterostructures (Fig. 2). Qualitatively these images are very similar to those obtained previously [4,10,11], where they were associated with bunches of misfit dislocations. It should be noted that in both structures the EBIC images obtained in the same place at different energies reveal practically the same structure (Fig. 3), although the contrast value essentially depends on E_b. At 90 K, the maximum cross-hatch EBIC contrast was observed at 15–20 keV and at such beam energies it reaches a value of about 2–4% for as-grown samples and of 1–2% for annealed ones. With temperature increase from 90 K to room temperature the contrast in both types of samples decreases 2–3 times. No cross-hatch contrast was observed at $E_b < 10$ keV.

If the cross-hatch pattern observed indeed is associated with bunches of misfit dislocations, such bunches should be located inside the graded SiGe layer, at least in as-grown structure, and their contrast dependence on E_b could be estimated using the Donolato model [16] and the effective depletion region width obtained by fitting the data presented in Fig. 1. The results obtained for dislocations located near the constant SiGe/graded SiGe interface ($1.1\,\mu$m), in the middle of graded SiGe layer ($1.45\,\mu$m) and at the graded SiGe/buffer layer interface ($1.7\,\mu$m) are shown in Fig. 4. As follows from these results, the contrast should monotonically increases with E_b and a relation between its values at 20 and 10 keV should exceed 20 for bunches located at the interface between graded and constant SiGe layers and should be even large for deeper bunches. In the samples studied this relation did not exceed 3–4 for annealed samples and 4–5 for as-grown ones.

Besides, the maximum density of such extended defects under an assumption that they are located inside the graded SiGe layer and that they totally determine the effective diffusion length could be estimated from the contrast value measured at 10 keV and the effective diffusion length. Such estimations were carried out and gave for a defect density a value of about $1/(6 \cdot L^2)$. For $L = 1.5\,\mu$m it is of about $10^7\,\mathrm{cm}^{-2}$ that gives for the distance between extended defects revealed in the EBIC mode a value of $10\,\mu$m, comparable with that seen in Fig. 2. But in this case about 2 times decrease of contrast after annealing should lead to a noticeable increase in L value that is not the case. Small L dependence on annealing could be explained taking into account the highly doped substrate effect but in this case

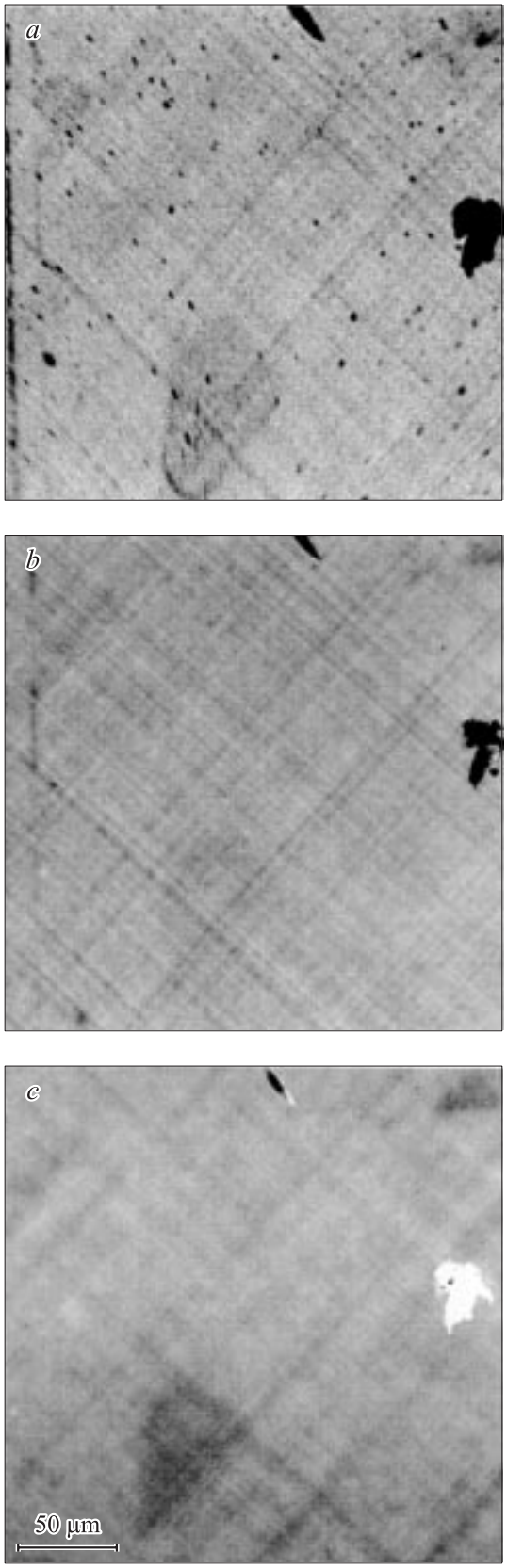

Figure 3. EBIC micrographs of annealed sample obtained at 90 K at $E_b = 10$ (*a*), 20 (*b*) and 30 keV (*c*), respectively. The micrographs were obtained on the same sample region.

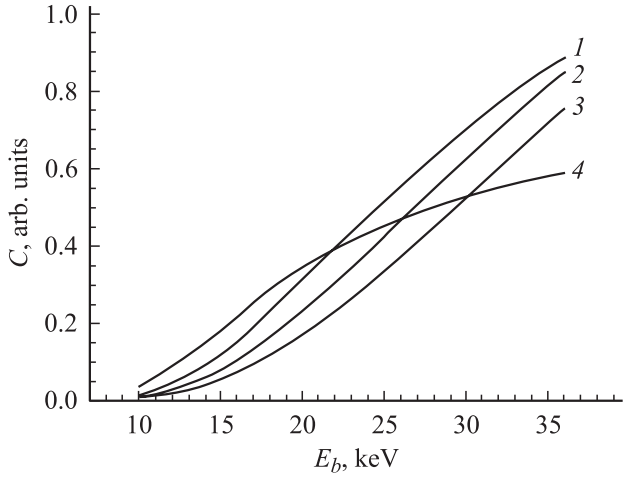

Figure 4. Calculated contrast dependences on E_b for misfit dislocations located at the depth 1.1 (*1*), 1.45 (*2*), 1.8 (*3*) and $0.6\,\mu$m (*4*).

the distance between extended defects should be larger than $10\,\mu$m, i.e. larger than the mean distance between dark lines on the experimental images. It should be noted that the misfit dislocations between bunches should be also taken into account in L calculations that should lead to a additional increase of calculated distance between the dark lines seen in the EBIC mode.

Thus, the problems is that to explain the contrast observed at 10 keV by defects located inside the graded SiGe layer rather high recombination strength for the defects should be assumed while the total defect concentration estimated from the effective diffusion length is limited by a value of about $10^{14}\,\mathrm{cm}^{-3}$ that in turn leads to a small defect density. Under assumption that the defects determining the observed cross-hatched image are located closer to the surface than the graded SiGe layer their recombination strength for the same contrast value could be smaller (see curve *4* in Fig. 4 that show an increase in the contrast at small E_b for defects located closer to the surface). Thus, an assumption that the defects responsible for the EBIC cross-hatch image are located closer to the depletion region allows to explain the contradiction between the effective L value and the EBIC contrast of extended defects and also the dependence of EBIC contrast on E_b. Thus, although the misfit dislocation bunches could not be totally excluded as a reason for the cross-hatch image observed, some additional defects located at a smaller depth should be looked for to explain the EBIC contrast.

It seems that threading dislocations could be excluded as such defects because their density is much lower than that of misfit ones and no reasons to assume that their electrical activity is much higher than that of misfit dislocations. The role of such defects could play dislocation trails, i.e. some specific defects formed behind moving dislocations in the dislocation slip planes. Indeed, such defects provide the noticeable EBIC contrast even in Si deformed in clean conditions, when the dislocation contrast is below the detectivity limit [13,14]. These defects could be revealed by chemical etching [15]. The dislocation trail contrast increases with a number of dislocations moving in the neighboring slip planes, therefore the dark regions in the EBIC micrographs could be associated with inhomogeneities in a number of moving threading dislocation and therefore their position could coincide with that of misfit dislocation bunches. And at last, such assumption allows to explain the decrease of EBIC contrast after at 800°C annealing because, as shown in [14], the EBIC contrast associated with dislocation trails annealed at 800–850°C. The absent of cross-hatched contrast at energies lower than 10 keV could be easily explained taking into account that, when the excess carriers are mainly created inside the depletion region, the contrast should strongly decrease (Fig. 4) and could not be detected by our setup. Thus, the dislocation trails could not be revealed at depth smaller than about $0.4-0.5\,\mu$m even if they preserve their recombination activity in this region. It should be also mentioned that dislocation trails give negligible diffuse contrast in the transmission electron microscope [15] therefore it is rather difficult to separate them from threading dislocations to check if they really exist in the structures under study.

4. Conclusion

Thus, the analysis of EBIC images obtained at different beam energies shows that misfit dislocation bunches in the graded SiGe layer could not explain the contrast dependence on E_b and the observed contrast values at low beam energies. Therefore, at least a part of cross-hatch contrast should be associated with other defects located at the smaller depth. It is shown that dislocation trails could play a role of such defects.

The authors would like to thank N.A. Yarykin for helpful discussions. This work was partially supported by the Russian Foundation for Basic Research (Grant 05-02-17730-a) and by the Silicon Wafer Engineering and Defect Science I/U CRC program under NSF grant EEC-9726176.

References

[1] M.L. Lee, E.A. Fitzgerald, M.T. Bulsara, M.T. Currie, A. Lochtefeld. J. Appl. Phys., **97**, 011 101 (2005).
[2] J.W. Matthews, A.E. Blakeslee. J. Cryst. Growth, **27**, 118 (1974).
[3] B. Samavedam, W.J. Taylor, J.M. Grant, J.A. Smith, P.J. Tobin, A. Dip, A.M. Phillips, R. Liu. J. Vac. Sci. Technol. B, **17**, 1424 (1999).
[4] L.M. Giovane, H.-C. Luan, A.M. Agarwal, L.C. Kimerling. Appl. Phys. Lett., **78**, 541 (2001).
[5] J.G. Fiorenza, G. Braithwaite, C.W. Leitz, M.T. Currie, J. Yap, F. Singaporewala, V.K. Yang, T.A. Langdo, J. Carlin, M. Somerville, A. Lochtefeld, H. Badawi, M.T. Bulsara. Semicond. Sci. Technol., **19**, L4 (2004).

[6] G. Eneman, E. Simoen, R. Delhougne, P. Verheyen, R. Loo, K. De Meyer. Appl. Phys. Lett., **87**, 192 112 (2005).
[7] S.H. Olsen, A.G. O'Neill, D.J. Norris, A.G. Cullis, N.J. Woods, J. Zhang, K. Fobelets, H.A. Kemhadjian. Semicond. Sci. Technol., **17**, 655 (2002).
[8] H.J. Leamy. J. Appl. Phys., **53**, R51 (1982).
[9] E.B. Yakimov. Izv. RAN, ser. fiz., **56** (3), 31 (1992). [In Russian, Transl. in Bull. Rus.Acad. Sci., **56** (3), 312 (1992)].
[10] X.L. Yuan, T. Sekiguchi, S.G. Ri, S. Ito. Appl. Phys. Lett., **84**, 3316 (2004).
[11] X.L. Yuan, T. Sekiguchi, J. Niitsuma, Y. Sakuma, S. Ito, S.G. Ri. Appl. Phys. Lett., **86**, 162 102 (2005).
[12] M. Kittler, C. Ulhaq-Bouillet, V. Higgs. Mater. Sci. Eng. B, **24**, 52 (1994).
[13] O.V. Feklisova, E.B. Yakimov, N. Yarykin, B. Pichaud. J. Phys.: Condens. Matter, **16**, S201 (2004).
[14] O.V. Feklisova, B. Pichaud, E.B. Yakimov. Phys. Status Solidi A, **202**, 896 (2005).
[15] I.E. Bondarenko, V.G. Eremenko, B.Ya. Farber, V.I. Nikitenko, E.B. Yakimov. Phys. Status Solidi A, **68**, 53 (1981).
[16] C. Donolato. Semicond. Sci. Technol., **7**, 37 (1992).

Редактор Л.В. Беляков